Effect of a DC electric field on a meniscus in a square groove

Nicolas Cardin, Laurent Davoust, Stéphane Lips, Samuel Siedel, Mostafa El Mehdi Brik, Jocelyn Bonjour

EFFECT OF A DC ELECTRIC FIELD ON A MENISCUS IN A SQUARE GROOVE

Nicolas Cardin[1,2], Laurent Davoust[2,*], Stéphane Lips[1], Samuel Siedel[2], Mostafa El Mehdi Brik[1], Jocelyn Bonjour[1]
[1]Univ Lyon, CNRS, INSA-Lyon, Université Claude Bernard Lyon 1, CETHIL UMR5008, F-69621, Villeurbanne, France
[2]Univ. Grenoble Alpes, CNRS, Grenoble-INP, SIMaP, F-38000, Grenoble, France

---

Abstract

The present study aims at investigating the deformation of a liquid-gas meniscus across a square groove when submitted to an electric field. Two numerical methods are developed: a first one (in-house) consists in solving the strong coupling between the Laplace-Young equation and the Laplace equation for the electric potential; the latter equation being required to get the distribution of the normal electric stress along the meniscus while the first equation is used to calculate the meniscus shape. The Laplace-Young equation is accordingly modified in order to take into account the added contribution of the normal electric stress. A second method based on the phase-field approach is developed for sake of comparison. The results demonstrate a fair agreement between both methods: the electric stress is found to be mostly focused on the top edges of the side walls, which pulls up the interface and yields higher curvatures for a same pressure jump. The in-house method is found to be significantly fast and to accommodate well with realistic boundary conditions, compared to the phase-field method which does not comply with the contact angle. The results, as obtained from the in-house method, are analysed based on non-dimensional numbers whose respective effects on the shape of the interface are properly investigated. A significant impact of the electric field near the triple contact line and at the centre of the groove is made evident. These effects can be described by considering an apparent angle near the triple contact line, or by considering the elevation of the meniscus centre. These results can be used in order to optimise an electro-capillary enhanced structure whose groove geometry is given.

Keywords: Meniscus; Capillary limit; Electrohydrodynamics; Contact angle

---

* Corresponding author: laurent.davoust@simap.grenoble-inp.fr, Phone: +33-47-682-52-06

1. INTRODUCTION

The coupling of an electric field with a low conductivity dielectric liquid is often referred to as electrohydrodynamics (EHD). There are many potential benefits of using EHD such as micropumping for cooling in microelectronics (Darabi and Wang, 2005), micromixing for biochemical developments (Siva Kumar Gunda *et al.*, 2012; Davoust *et al.*, 2013; Sharma *et al.*, 2015), drop motion for cooling, display or biological applications (Pollack *et al.*, 2000; Bahadur and Garimella, 2008; Cheng and Chen, 2010), shape deformation of meniscus and drops for optical or biological applications (Cheng *et al.*, 2006; Ko *et al.*, 2009; Malk *et al.*, 2011; Theisen and Davoust, 2012, 2015). Different actuation mechanisms based on EHD can be developed depending on whether a dividing interface is present or not, depending on the electrical properties of the fluids involved (electrical conductivity, dielectric permittivity), on the frequency (DC regime vs AC regime, voltage period to relaxation time ratio…), on the uniformity of the electric field...etc.

The need to enhance the performance and the robustness of stratified two-phase systems currently leads to the development of innovative methods. In such systems, one of the main limitation is the pumping of the fluid, such as for instance, heat pipes (Faghri, 1995) or lab-on-a-chips (Haeberle and Zengerle, 2007). Here again, EHD can be hoped to deliver substantial benefits. For instance, EHD is already used to improve heat transfers in thermal systems (Siedel *et al.*, 2011; Cotton *et al.*, 2012; Diao *et al.*, 2015; Mancio Reis *et al.*, 2015; Quan *et al.*, 2015). The use of electrical body forces such as electrophoretic forces requires the presence of electrical charges inside the fluid media and eventually a dielectric coating on the electrodes in order to avoid the creation of damaging electrical density currents. For this reason, we focus, in the present paper, on interfacial EHD (often referred to as Taylor-Melcher EHD): in this case, the electric charges in the volume phases vanish while the presence of a dividing interface between them leads to a jump in the electrical properties and to the presence of a surface charge density. This causes a surface electric stress to arise (Castellanos, 1998), which can be used to enhance the pumping of liquid along a micro-channel, provided the viscous shear stress is large enough. Typically, interfacial EHD can also be used in order to improve the performance of thermal systems such as grooved heat-pipes, the latter being passive heat transport devices made of a sealed cavity filled by a two-phase working fluid. Past experiments have demonstrated the possibility to use EHD inside heat pipes (Jones, 1973; Loehrke and Sebits, 1975; Cooper, 1990; Bryan and Seyed-Yagoobi, 1997). However due to the various geometries studied and the presence of phase change in heat pipes (condensation / vaporization), the detailed nature of EHD (conductive vs inductive regimes) was not really made clear. Several numerical models in the literature aim at explaining or describing EHD effects on a liquid ridge along the capillary groove of a planar heat pipe. Suman (2006) and more recently, Saad *et al.* (2017), developed a model taking into account both hydrodynamics and heat transfer along a capillary groove submitted to a DC electric field. However, these models deal with the pumping ability of the tangent electric stress but do not take into account the unavoidable deformation of the liquid-gas interface caused by the normal electric stress. Hence, there is still need for developing robust numerical methods with small enough computational (CPU) time and a strong ability to comply with coupled boundary conditions at a EHD-induced surface deformation. To address this issue, the more appropriate configuration seems to be a square groove, or an array of square grooves, due to its relevance to grooved heat-

pipes and the possibility to consider contact line pinning at the top edges of the groove (Hallinan *et al.*, 1998; Chang and Hung, 2017).

The present article investigates the way a meniscus is deformed across a rectangular groove when it is submitted to a normally applied DC electric field. Focus is definitely put on the normal component of the (jump) momentum balance at the liquid/gas interface. This normal balance is found to be nothing but an extended version of the Laplace-Young equation. Two numerical methods are presented: the first one is based on an iterative method to solve for the coupling between the Laplace-Young equation and the Laplace equation for the electric potential while the second one is based on the phase-field approach. The groove is filled with a liquid whose conductivity is supposed to be significantly larger than that of the gas. The gas medium can be considered as a perfect dielectric medium.

2. WORKING GEOMETRY AND MODELING

2.1. Working geometry

In this study, a sealed cavity formed by two horizontal plates is considered (Fig. 1a). The top plate is flat and connected to a high voltage while the bottom plate is grooved and connected to ground. The capillary structure along the lower plate is an array of axial square grooves filled with a working liquid. Fig. 1b represents the elementary working geometry under consideration in this paper. The configuration is viewed as 2-D and the length of the grooves is consistently considered infinite. The top edges of the grooves are assumed to be rounded at the microscale of the contact line with a very small radius of curvature (radius r, see Fig. 1b). The effect of this last parameter will be discussed in details in section 3.1.4. This approximation is consistent regarding the current manufacturing methods.

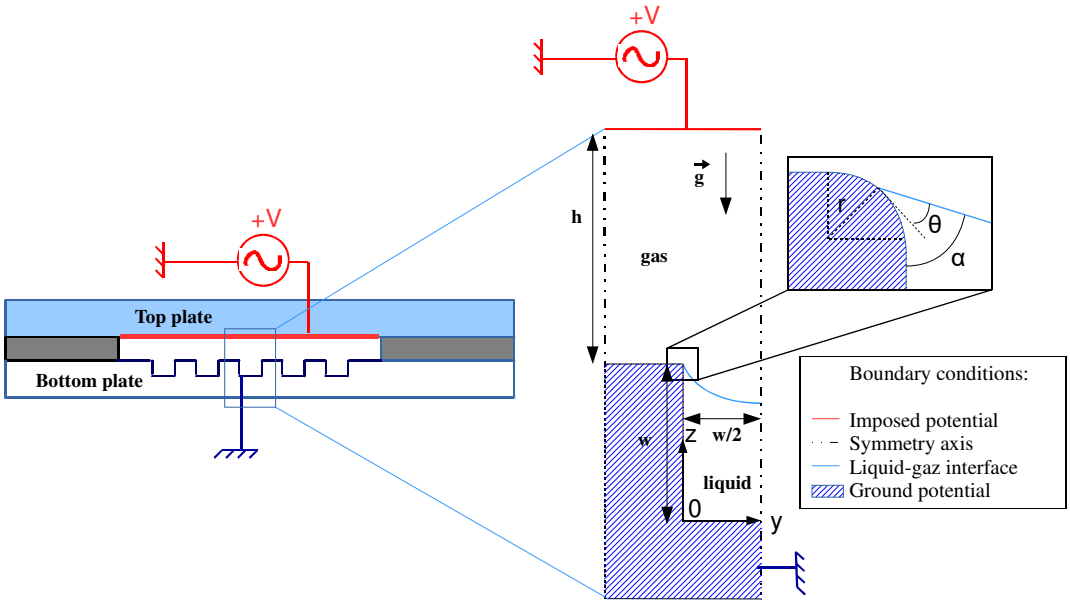

Overall geometry Close-up of a groove cross-section and meniscus

Fig. 1. 2-D configuration under consideration.

2.1. Electrostatics and subsequent stress

In order to evaluate the electric field inside the working geometry, the absence of free electric charges is

consistently assumed. This assumption is indeed valid when dielectric fluids, such as liquids based on fluorocarbons or any kind of fluids with a large electric charge relaxation time, are used in AC regime. The electric charge relaxation time is defined as the ratio between the electric permittivity and the electric conductivity ($\tau = \varepsilon/\sigma_e$). If it is sufficiently larger than the period of the applied AC electric signal, then the only non-vanishing electric charges are found to be focused on the dividing interfaces. For example, τ is reported to be about 2.1 s for R113 (Zaghdoudi and Lallemand, 2000), and about 150 s for FC-72 (Di Marco, 2012). It can be noted that for practical reasons this assumption could be questionable when using fluids with a low electric charge relaxation time (semiconducting fluids). The second principal curvature of the interface, as defined along the x-axis of the groove, is assumed negligibly small compared to the first principal curvature, defined across the groove (y-axis), which is consistent with the assumption of a two-dimensional layout. As a consequence, the electric field is evaluated by solving the Laplace equation:

$$\vec{\nabla}.(\varepsilon\,\vec{\nabla}\mathrm{V}) = 0, \tag{1}$$

where ε is the medium permittivity and V is the electric potential. A high voltage potential $\mathrm{V} = \mathrm{V}_0$ is imposed at $z = \mathrm{h} + \mathrm{w}$ (upper plate) and the groove is connected to ground. Two symmetry axes are defined along $\mathrm{y} = \pm\mathrm{w}/2$ (Fig. 1b), which leads to the boundary condition: $\varepsilon\,\vec{E}.\vec{n} = 0$. The value of the electric field should not exceed the value of the maximal electric field the fluids involved can sustain before dielectric breakdown, the latter being essentially driven by the geometry and the dielectric strength of the fluids. As illustrated by the literature, this requirement is experimentally fulfilled in presence of electric fields for some usual (two-phase) fluorocarbon fluids(see e.g. Ogata and Yabe, 1993; Liu et al., 2006; Di Marco et al., 2013; Siedel et al., 2016; Cardin et al., 2018).

The effect of EHD depends on the terms present in the Maxwell tensor, as derived from the Korteweg-Helmholtz force (Stratton, 1941):

$$\vec{\mathrm{F}} = \mathrm{q}\vec{\mathrm{E}} - \frac{1}{2}\nabla\left(\varepsilon - \rho\frac{\partial\varepsilon}{\partial\rho}\Big|_{\mathrm{T}}\right)\vec{\mathrm{E}}.\vec{\mathrm{E}}, \tag{2}$$

where q is the volume charge density, ρ the density of the fluid, ε the electric permittivity, T the temperature and $\vec{E}$ the electric field. In the present study, the Coulombic term which scales linearly with the charge density q in Eq. (2) is vanishing (very large charge relaxation time). The second term is the dielectric force which depends on the non-uniformity of the electric permittivity inside the medium. The term depending on the variation of the electric permittivity as a function of the fluid density represents the electrostrictive force; it can be neglected in isothermal conditions (Chang, 2010), which is consistent here since the focus is put on a cross section of the groove.

The electric stress is then evaluated by calculating the jump in the Maxwell tensor at the interface between the two media (Castellanos, 1998). The resulting electric stress can be decomposed into two components at and along the interface, namely a normal stress,

$$\tau_n = \frac{\varepsilon_g}{2}(E_{g,n}^2 - E_{g,t}^2) - \frac{\varepsilon_l}{2}(E_{l,n}^2 - E_{l,t}^2), \quad (3)$$

and a tangential stress,

$$\tau_t = (\varepsilon_g E_{g,n} - \varepsilon_l E_{l,n}) E_t, \quad (4)$$

where ε_i is the dielectric permittivity of the liquid (i=l) and gas (i=g) phases, $E_{i,n}$ and $E_{i,t}$ are the normal and tangential components of the electric field at and along the interface, together with the condition that $E_{l,t} = E_{g,t} = E_t$. The symbols n and t denote the normal and tangential components. The normal unit vector $\vec{n}$ at the interface is directed from liquid to gas phases.

The normal stress is commonly involved in the topic of EHD-driven surface deformation, especially when considering electrosprays (Shin *et al*., 2004; Atten, 2012), liquid columns (Pellat, 1896; Jones, 2005) or moving droplets in a transverse electric field (Mandal and Chakraborty, 2017; Santra *et al*., 2018). All these studies show the ability of the normal electric stress to enhance wetting or to assist the capillary stress defined as the product of the surface tension with the mean surface curvature.

2.2. Deformation of the interface

The studied geometry is a 2-D cross section of the system described in Fig. 1. As usual in grooved heat-pipes, the groove under consideration here has a finite length and so, exhibits two expansion volumes at its ends. As a consequence, there is no reason to argue mass conservation in order to evaluate the meniscus shape along the groove. Instead, a control parameter is considered to monitor the shape of the interface, namely the curvature at the centre of the interface. Assuming that the normal component of the viscous stress is negligible, the local (mean) curvature is linked to the pressure jump at the interface by way of the Laplace-Young equation corrected by the normal electric stress:

$$\Delta P = (P_g - P_l) = \sigma\kappa + \tau_n, \quad (5)$$

where σ is the surface tension between the working fluids, κ is the mean curvature of the interface, τ_n is the normal electric stress and $(P_g - P_l)$ is the pressure jump at the interface. The pressure difference between any point along the interface and the centre of the interface depends on the gravity:

$$\Delta P(y) = g\Delta\rho(y - y_0) + \Delta P(y_0), \quad (6)$$

where $\Delta\rho$ is the difference between the fluid phases densities, y is the coordinate across the groove (Fig. 1b) and y_0 is the transverse location of the centre of the meniscus: $y_0 = w/2$. For a given fluid and the geometry considered here, the surface shape can be seen as governed by the pressure difference at the centre of the interface. Combining Eqs. (5)-(6), the mean curvature along the meniscus can be expressed as,

$$\kappa(y) = \kappa_0 - \frac{\tau_n(y_0) - \tau_n(y) - g\Delta\rho z}{\sigma}, \quad (7)$$

or alternatively as a function of the slope of the meniscus,

$$\kappa(y) = \cos\phi \frac{d\phi}{dy}, \tag{8}$$

with ϕ, the angle between the vertical axis and the normal unit vector at the interface.

By considering Eqs. (6), (7) and (8), the variation of ϕ along the interface can be expressed as follows:

$$\frac{d\phi}{dy} = \frac{\kappa_0 + \frac{z(y)\Delta\rho g}{\sigma} - \frac{\tau_n(0) - \tau_n(y)}{\sigma}}{\cos(\phi(y))}. \tag{9}$$

The meniscus shape can be calculated taking account of the boundary conditions, namely the curvature $\kappa(y = w/2) = \kappa_0$, at the centre of the interface, and the contact angle at the triple contact line (TCL), θ. The boundary condition is written at the TCL so as to match the contact angle at the rounded edge (Fig. 1b), which leads to $\phi = \frac{\pi}{2} - \text{acos}\left(\frac{y_c}{r}\right) - \theta$, with r, the radius of the edge at the top of the side walls, and y_c, the position of the TCL.

2.3. Dimensionless mathematical model

The previous equations can be better written using dimensionless numbers. The Laplace equation for the electric potential is revised as follows,

$$\vec{\nabla}.(\varepsilon^*\vec{\nabla}V^*) = 0, \tag{10}$$

considering the non-dimensional variables, $\varepsilon^* = \frac{\varepsilon_l}{\varepsilon_g}$ and $V^* = \frac{V}{V_0}$, and the width of the groove, w, to be the length scale. Dirichlet conditions are imposed at the top plate, with $V^*(z^* = 1 + h^*) = 1$, and at the lower plate, with $V^* = 0$. A symmetry condition about the longitudinal mid-axis of the groove is taken into account by writing that: $\varepsilon^*.\ \overrightarrow{E^*}(y^* = \pm\frac{1}{2}).\vec{n} = 0$. The electric stresses write accordingly,

$$\tau_n^* = \frac{Bo_e}{2\varepsilon^* h^*}(E_{g,n}^{2^*} - E_{g,t}^{2^*}) - \frac{Bo_e}{2h^*}(E_{l,n}^{2^*} - E_{l,t}^{2^*}), \tag{11}$$

$$\tau_t^* = \frac{Bo_e}{h^*}\left(E_{l,n}^* - \frac{E_{g,n}^*}{\varepsilon^*}\right)E_t^*, \tag{12}$$

with $\tau^* = \frac{\tau}{\sigma}w$, $\varepsilon^* = \frac{\varepsilon_l}{\varepsilon_g}$, $E^* = \frac{E}{V}w$ and the electric Bond number defined as, $Bo_e = \frac{\varepsilon_l V^2}{\sigma w}$. The dimensionless pressure jump is now written as,

$$\Delta P^* = \kappa^* + \tau_n^*, \tag{13}$$

with $\Delta P^* = \Delta P\frac{w}{\sigma}$ and $\kappa^* = \kappa w$. The dimensionless elevation of the interface writes as:

$$z^* = \frac{\kappa^*(0) - \kappa^*(y^*) - \left(\tau_n^*(0) - \tau_n^*(y^*)\right)}{Bo}, \tag{14}$$

with $z^* = \frac{z}{L}$ and the Bond number defined as, $Bo = \frac{\Delta\rho g w^2}{\sigma}$.

The dimensionless variation of ϕ can therefore be expressed as follows:

$$\frac{\mathrm{d}\phi}{\mathrm{d}y^*} = \frac{\kappa_0^* + \mathrm{Bo}\, z^* - \left(\tau_n^*(y_0^*) - \tau_n^*(y^*)\right)}{\cos(\phi(y^*))}. \tag{15}$$

The curvature of the meniscus at the centre is prescribed, which leads to $\kappa^*\left(y^* = \frac{1}{2}\right) = \kappa_0^*$, and the contact angle is imposed with the following condition $\phi = \frac{\pi}{2} - \mathrm{acos}\left(\frac{y_c^*}{r^*}\right) - \theta$.

The dimensionless numbers previously defined are described in Table 1.

Table 1. Non-dimensional numbers and variables.

Bo	$\frac{(\rho_2 - \rho_1)gw^2}{\sigma}$	Bond number
Bo_e	$\frac{\varepsilon_l V^2}{\sigma h}$	Electric Bond number
h^*	h/w	gas spacing
r^*	r/w	edge radius
x^*, y^*, z^*	$\frac{x}{w}, \frac{y}{w}, \frac{z}{w}$	spatial coordinates
κ^*	κw	curvature
ΔP^*	$\frac{\Delta P w}{\sigma}$	pressure jump
τ_n^*	$\frac{\tau_n}{\sigma} w$	electric stress
ε^*	$\frac{\varepsilon_l}{\varepsilon_g}$	electric permittivity

The Bond number represents the balance between the capillary force and the gravity force. It tends to zero when gravity effects become negligible due to the small length scale. The electric Bond number represents the balance between the normal electric stress and the capillary stress. The dimensionless forms of the pressure jump and the normal electric stress represent respectively the ratio of the pressure jump over the maximal capillary pressure and the ratio of the normal electric stress over the maximal capillary pressure. The dimensionless electric permittivity is the ratio of the liquid to gas permittivities; its value gives information on the medium where the electric field becomes significant.

3. NUMERICAL PROCEDURE

The mathematical model, based on Eq. (10) and Eq. (15), together with the previously-defined boundary conditions, enables to analyse the effect of the electric field on the meniscus in a square groove as long as the assumptions are respected (no free charge, no tangential stress, infinite curvature along the groove). A two-way coupling must be emphasized: the evaluation of the electric potential depends on the elevation of the liquid-gas interface, while the calculation of the latter depends on the electric potential map. In order to address this coupling, two different approaches are developed. The in-house method (SLASH) focuses on this strong coupling but the flow is disregarded and the problem refers to electrohydrostatics (EHS) alone. The second method based on phase field includes the Navier-Stokes equations together with the normal and tangential momentum balances at the interface. The comparison between the two methods should allow us to validate the

first method based on EHS.

3.1. Iterative method as developed in SLASH

An iterative method is developed in order to enable a fast and accurate evaluation of the interface shape at equilibrium. A similar method was developed by Buehrle *et al.* (2003) to evaluate the effect of the electric field on a contact angle. In a first stage, the electric potential is solved using the finite element method-based software *Comsol Multiphysics*. In a second step, the electric potential distribution is exported from COMSOL to MATLAB environment. The (jump in the) normal electric stress, τ^*_n, is calculated at the location of the liquid-gas interface, the latter of which is updated by solving the Laplace-Young equation (15) from a shooting-method. In a third step, the newly calculated elevation of the liquid-gas interface is exported to COMSOL and the electric potential distribution is updated by solving again the Laplace equation…etc. This iterative process is performed as long as the numerical error on the surface elevation is not small enough. This methodology is referred to as SLASH for "Steady Laplace Analytic Solution for Heat pipe.

3.1.1. Electric quantities

Fig. 2 shows the distribution of the electric field in presence of the interface for $Bo = 0$, $Bo_e = 5$, $h^* = 3$, $\varepsilon^* = 2$ and considering a cylindrical interface with $\kappa_0^* = 0.25$.

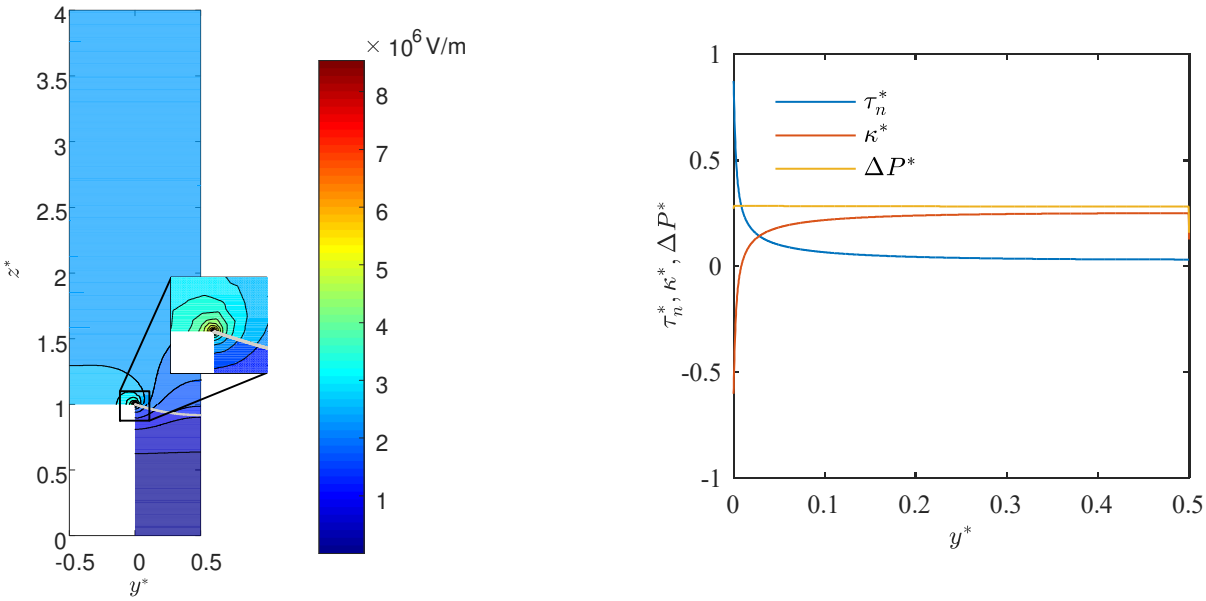

Fig. 2. Colormap of the electric field (a) and normal electric stress (b) for $\mathrm{Bo} = 0.1$, $\mathrm{Bo_e} = 5$, $\mathrm{h}^* = 3$, $\varepsilon^* = 2$ and $\kappa_0^* = 0.25$.

The results show that the electric field inside the liquid phase is much smaller than the one in the gas phase, and that the electric field is consistently focused near the edges of the groove. The electric stress being consequently focused on the edges, as well, a significant shape deformation of the interface is expected near the TCL. The evolution of the normal electric stress τ_n^* along the interface is presented on Fig. 2b. Compared to the capillary stress κ^*, the normal electric stress τ^* is found small all along the interface except near the edge of the groove where it increases very significantly. This local effect is due to the edge which behaves as a Taylor cone. The roundness of the edge enables to avoid the arising of a singular electric stress. For this configuration, the maximal value of the electric field along the edge is proportional to $r^{*-1/3}$ (see parametric analysis in section 3.1.4).

3.1.2. Calculation of the shape of the meniscus

Given the evolution of the normal electric stress along the interface, a shooting method is used to evaluate the shape of the interface. This shape is determined by solving Eq. (15), starting from the centre of the groove where axial symmetry is secured and where an initial curvature κ_0 is imposed as a first boundary condition.

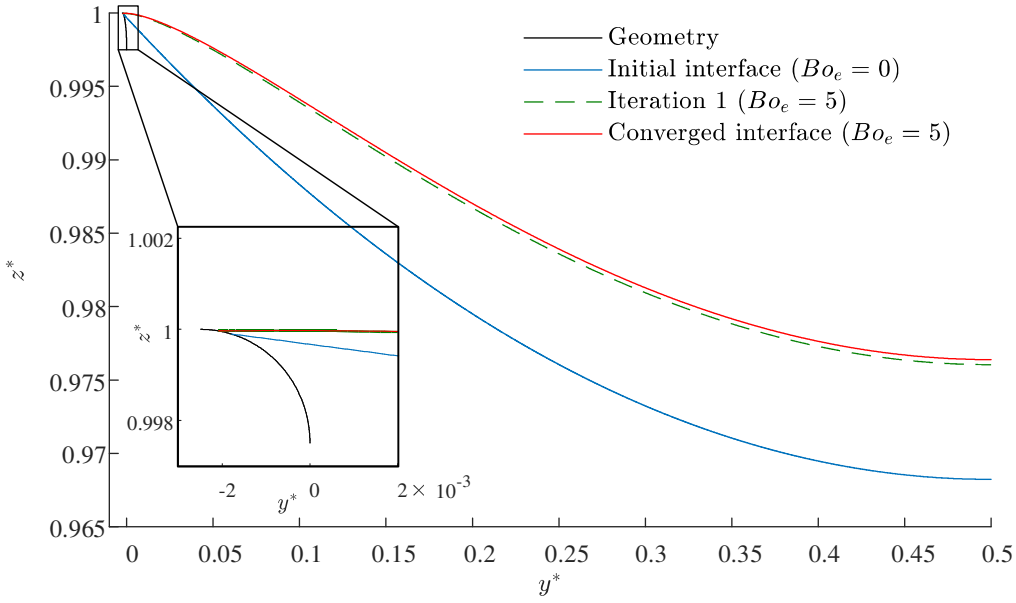

Fig. 3. Deformation of the meniscus shape in presence of an electric field for $\mathrm{Bo} = 0.1$, $\mathrm{Bo_e} = 5$, $\mathrm{h}^* = 3$, $\varepsilon^* = 2$ and $\kappa^* = 0.25$.

The shooting method is used to take account of the boundary condition at the side wall. By doing so, the elevation z_0 of the centre of the interface is adjusted along the vertical axis. For each iteration step, the value of z_0 is modified to comply with the wetting angle θ at the rounded edge. Doing so, the electric field must be updated due to the need for updating the jump condition on the electric stress at the newly calculated interface. The definitive interface is found after a sufficient number of iterations, i.e. when the numerical error on the elevation is found small enough (section 3.1.). It is worthy to note that the initial shape of the interface is analytically calculated in the case of a liquid-gas interface with no electric field applied. Fig. 3 represents an example of the evaluation of the interface for a curvature at the centre, $\kappa^* = 0.25$, and a given contact angle between the solid edge and the liquid-gas interface. The main deformation of the interface is focused near the edge where the electric field is also focused. It impacts the elevation of the meniscus at the centre of the groove.

3.1.3. Convergence of the solution

The SLASH methodology is based on an iterative procedure with the evaluation of the electric field as the first step of a numerical loop and the evaluation of the meniscus shape as a second step. In order to reach the steady solution, a convergence condition is introduced which relies on the deformation of the meniscus at the centre and near the TCL. The deformation near the TCL can be described by the introduction of the apparent angle, defined as the angle between the vertical axis and the tangent vector along the interface at the TCL (Fig. 1). But a criterion only based on this angle is not relevant for the accurate evaluation of the meniscus elevation at the centre. Therefore, one introduces a convergence criteria based on the maximal value among all the differences between the two last successive elevations of the points defined along the discretised interface, $\Delta z^* = \frac{\Delta z}{w}$. This maximal difference is submitted to the following convergence condition: Δz^*_{max} is set at 2.5×10^{-5}. Fig. 3 focuses on the meniscus shape at the edge during the iterative process of convergence, given a set of non-

dimensional numbers. Only few iterations are usually required to fulfil the convergence condition. In the present example, here, it can be noted that the first iteration and the converged solution are comparable because the electric field is mainly focused near the edge. Only few points near the TCL remain out of the convergence condition after a second iteration. Fig. 3 also displays a focus on the centre of the interface for the same set of non-dimensional numbers. The fast convergence of the solution after only a limited number of iterations suggests a significant robustness of the numerical method.

3.1.4. Sensitivity analysis on the radius of the rounded edge

The edge radius r^* is difficult to determine in a real experimental set-up. A sensitivity study is thus conducted to investigate the role of this parameter. Fig. 4 shows the meniscus shape dependence on the edge radius, with or without the electric field imposed. Because the curvature at the centre of the interface is given, the impact is more focused at the edge. Different values of r^* are considered. These values are small enough to consider the edge to be sharp from a mechanical point of view and therefore, the contact line is considered to be pinned at the edge. When no electric field is applied (solid lines), all interfaces exhibit the same slope close to the TCL (Fig. 4 close-up). The radius of curvature of the edge only affects the location of the TCL but the effect on the apparent angle remains negligibly small. This is particularly true for a non-dimensional radius smaller than $1/400$.

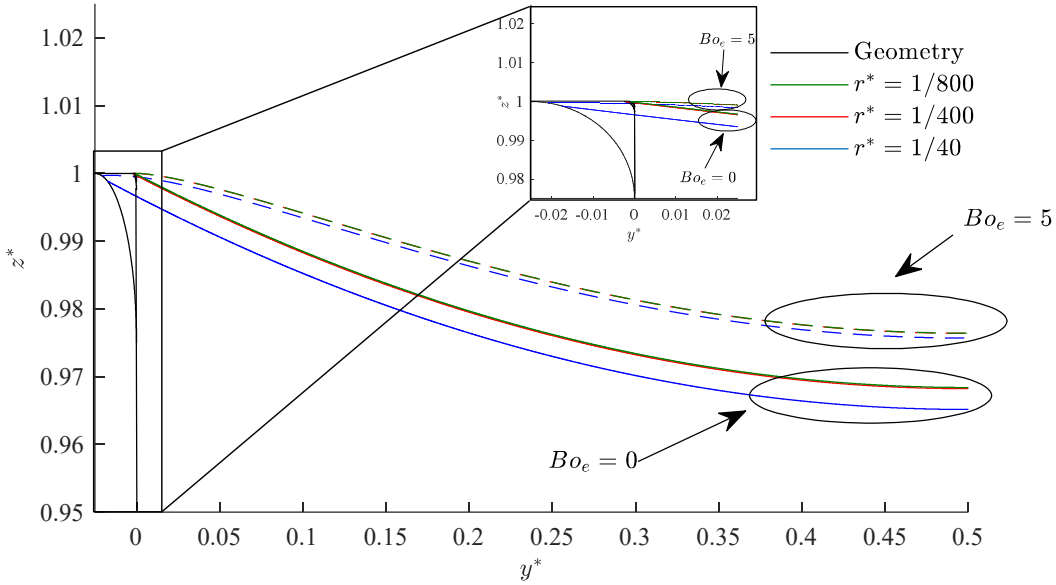

Fig. 4 Meniscus shape for different radii with a focus near the edge for $Bo = 0.1$, $Bo_e = 5$, $h^* = 1$ and $\kappa^* = 0.25$

In presence of an electric field (dashed lines), the change in the apparent angle becomes significant. The results show that all the three interfaces are almost the same in presence of an electric field for a given curvature at the centre of the interface (Fig. 4). The apparent angle and the pressure jump at the centre of the interface in presence of an electric field in the same conditions as before are displayed in Table 2.

Table 2. Effect of the radius of the fin edge on the pressure jump and the apparent angle for $Bo = 0.1$, $Bo_e = 5$, $h^* = 1$ and $\kappa^* = 0.25$

r^*	ΔP^*	α (°)
1/40	1.604	80.40
1/400	1.604	80.47

1/800	1.604	79.91

The variation of the non-dimensional radius has no significant impact on the pressure jump and a very low impact on the apparent angle (less than 1 degree). In the present configuration, the radius of the fin edge, r^*, can thus be considered only as a numerical parameter. In the following, r^* is then fixed to $r^* = 1/400$ as a good trade-off for taking benefit from the effect of the Taylor cone induced by the sharp edge but with still a reasonable mesh size. Moreover, note that a smaller radius reveals to be useless, because of its weak impact on the pressure jump and the apparent angle.

3.1.5. Sensitivity analysis on the contact angle

The (physicochemical) contact angle θ characterizes the competition between the three surface energies at the TCL. Depending on its value, the liquid is wetting (low contact angle, typically smaller than 90°) or non-wetting (high contact angle, typically larger than 90°). The apparent angle α is a geometric angle as described previously. In the absence of an electric field and when the gravitational force is negligible, the liquid-gas interface is a portion of circle. The apparent angle is thus independent of the contact angle:

$$\alpha = \mathrm{acos}(\kappa^*/2). \tag{16}$$

It can be noted that for a wetting fluid, the curvature κ is positive while it is negative for a non-wetting fluid. For a meniscus attached to the edge of a groove, the contact angle should not affect the evaluation of the apparent angle or the pressure jump. It will only affect the minimum and maximum possible values of the meniscus curvature. Table 3 summarizes the variation of the non-dimensional pressure jump at the centre of the interface and the variation of the apparent angle α for various θ. The results show no effect of the contact angle on these parameters. The contact angle θ can be considered as a numerical parameter which is chosen equal to 10° for positive curvatures and equal to 110° for negative curvatures.

Table 3. Effect of the contact angle on the pressure jump and the apparent angle for $Bo = 0.1$, $Bo_e = 5$, $h^* = 1$ and $\kappa^* = 0.25$

Θ (°)	ΔP^*	α (°)
10	1.604	80.47
20	1.604	80.36
30	1.604	80.36

3.2. Phase Field

In order to benchmark the method and the results described previously, a phase field approach is attempted. Phase field is commonly used to track the interfaces and to evaluate their shape (Chen, 2002). A great advantage of this methodology is its capability to evaluate the creation, the coalescence or the collapse of highly deformable inclusions. Moreover, phase-field was already used to evaluate the 3-D shape of a droplet pervaded by an electric field (Yang *et al.*, 2013). One of its main drawback is the calculation time, which stands as a major problem when designing a system. In the phase field method, the position of the interface is tracked by

introducing a characteristic function ψ defined on a fixed (eulerian) mesh:

$$\psi(n) = -\tanh\left(\frac{n}{\sqrt{2}W}\right), \qquad \text{with } \psi \in [-1,1], \tag{17}$$

with $\psi = -1$ in the gas phase, $\psi = 1$ in the liquid phase, $\psi = 0$ at the interface. The physical properties at the interface are weighted by the function ψ in order to take into account as much as possible their sharp changes across the interface. The symbol n is defined as the coordinate along the normal direction at the interface. The function ψ is transported by the fluid velocity according to:

$$\frac{\partial \psi}{\partial t} + \vec{U}.\vec{\nabla}\psi = 0. \tag{18}$$

Eq. (18) enables the resolution of the meniscus deformation. With this methodology, the initial position of the interface is given along the isovalue, $\psi = 0$. The function ψ is time-dependent, which can lead to rupture or reconnection of the interface in some cases. The normal unit vector at the interface is classically evaluated in the phase field method considering $\psi(n)$ to be an implicit function:

$$\vec{n} = \frac{\vec{\nabla}\psi}{\|\vec{\nabla}\psi\|}. \tag{19}$$

The transport equation could be written assuming the normal component of the velocity depends linearly on the curvature: $u_n = a - b\kappa$. This assumption can be used for important deformations (Sun and Beckermann, 2007) and leads to the following equation:

$$\frac{\partial \psi}{\partial t} + a\|\vec{\nabla}\psi\| + u_t.\vec{e_t}\vec{\nabla}\psi = b\left[\vec{\nabla}^2\psi + \frac{\psi(1-\psi^2)}{T^2} - \|\vec{\nabla}\psi\|\vec{\nabla}\left(\frac{\vec{\nabla}\psi}{\|\nabla\psi\|}\right)\right], \tag{20}$$

with T the thickness of the interface and (a,b) two numerical parameters corresponding respectively to the relaxation time of the director field and the interface. More details can be found in the literature (see e.g. Yue *et al.*, 2006 and Akhlaghi Amiri & Hamouda, 2013) on the calculation of the surface deformation and the implementation of the surface tension with the phase-field and FEM approaches. These parameters (a,b) only affect the transient regime, so that they are arbitrary chosen to ensure a fast convergence. In the present study, the phase field method is implemented using *Comsol-Multiphysics*. The electric field is calculated by using the same Eq.(1) for the electric potential as in the SLASH methodology and the Maxwell tensor is calculated on the entire liquid-gas domain. Simultaneously, the shape of the interface is calculated from the characteristic function ψ by solving the Navier-Stokes equations, with the Maxwell and the mechanical tensors, as well as the transport equation for ψ. The pressure jump as well as the symmetry condition are imposed at the centre of the interface. At the TCL, the boundary condition is ensured by adding a pointwise stress depending on the contact angle.

4. NUMERICAL RESULTS

The study is based on a fixed geometry with a 400x400 µm square groove. The gas spacing and the properties of the fluid are numerically modified to adjust the various dimensionless numbers. In order to compare the phase field method with the SLASH method, a set of parameters is fixed and the results as obtained from each methods are compared. The effect of the intensity of the electric field is studied from the electric Bond number Bo_e. The effect of the geometry and the properties of the fluids are investigated from the aspect ratio h^*, the Bond number Bo and the non-dimensional permittivity ϵ^*.

4.1. Effect of the electric Bond number

The effect of the intensity of the electric field on the shape of the interface depends on the electric Bond number. Because of the boundary conditions, the curvature at the centre of the interface is fixed for the SLASH methodology. In order to study the impact of the electric Bond number on different shape of the interface, a set of curvatures at the centre of the interface is studied. The others parameters remain fixed: $Bo = 0$, $h^* = 3$ and $\varepsilon^* = 2$. Fig. 5 essentially represents the variation of ΔP^*as a function of κ^* for two values of Bo_e. It also displays the relationship between ΔP^* and κ^* that can be found analytically for the case where no electric field is applied ($Bo_e = 0$). The pressure jump is chosen to represent the effect of EHD on the centre of the interface: the larger the electric Bond number, the larger the pressure jump. This effect is even more intense for high and negative curvatures at the centre of the interface. The results issued from phase field and SLASH methods are in very good agreement at the centre of the interface. Both methods can be used to evaluate the pressure jump at the interface. It must be emphasized that the maximum electrical bond number is limited by the dielectric strength of the working fluid. For instance, (Di Marco *et al.*, 2013) performed experiments with a Bo_e up to 9.5 using FC-72 and (Cardin *et al.*, 2018) reached Bo_e ranging from 3 to 50 with HFE-7100.

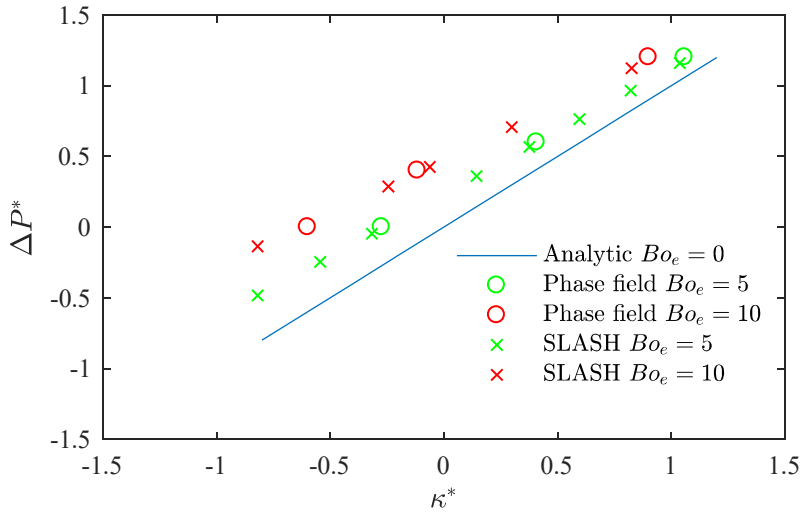

Fig. 5. Comparison of the phase field and SLASH for $h^* = 3$, $\varepsilon^* = 2$ and , $\mathrm{Bo} = 0$.

To describe the effect of the electric field near the TCL, the apparent angle is introduced. In order to benchmark the sensibility of the apparent angle as a function of the contact angle, the results issued from the different methods are compared in the absence of electric field. In this case, the value of the apparent angle is independent of the contact angle (16). Fig. 6 represents the variation of the apparent angle as a function of the contact angle between the liquid-gas interface and the solid edge. It can be noted that SLASH ensures an apparent angle independent of the contact angle as also predicted by the analytical solution in the absence of electric field, which is not the case with the phase field method.

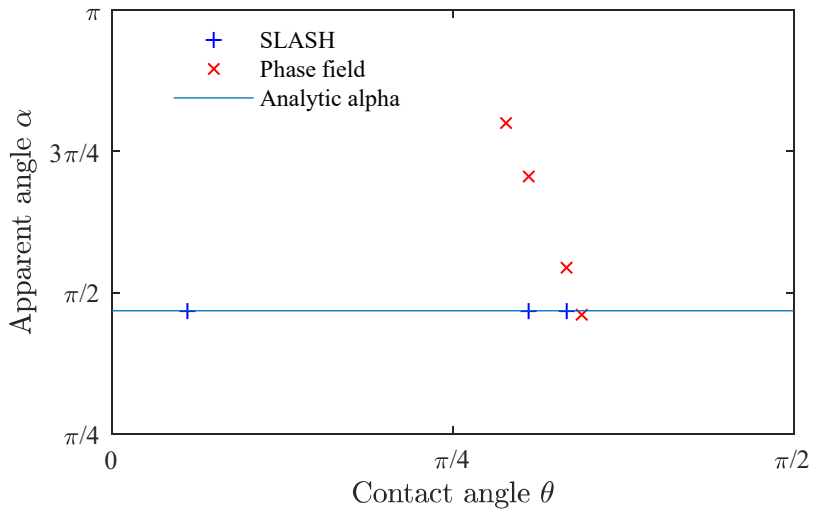

Fig. 6. Evaluation of the apparent angle for various contact angles with $Bo = 0$, $Bo_e = 0$, $\varepsilon^* = 2$, $\Delta P^* = 0.2$ and $h^* = 3$.

Near the edge, both methods deliver a different interface shape because of the different boundary conditions considered. The SLASH method imposes the contact angle at the edge whereas the phase field method imposes a stress near the TCL. This boundary condition reduces the capability of the phase field approach to estimate properly the apparent angle.

4.2. Effect of the gaseous gap on the normal electric stress

The parameter h^* is linked to the distance between the top electrode and the groove. This parameter has a significant impact on the electric field and thus on the distribution of the electric stress along the interface. Fig. 7 shows the deformation of the liquid-gas interface for various h^*, as evaluated with the methods presented previously. The dotted lines represent the solution obtained from the phase field method and the solid lines represent the results as obtained from SLASH method. When the gas spacing is reduced, the electric field is more focused near the edge. When the top electrode approaches the groove, the electric field increases at the TCL, which leads to a strong deformation of the interface. Thus, the parameter h^* has also a strong impact on the apparent angle. This effect is found more important with the phase field method but this is due to the bias imposed by this method. In the following, only the SLASH results are reported.

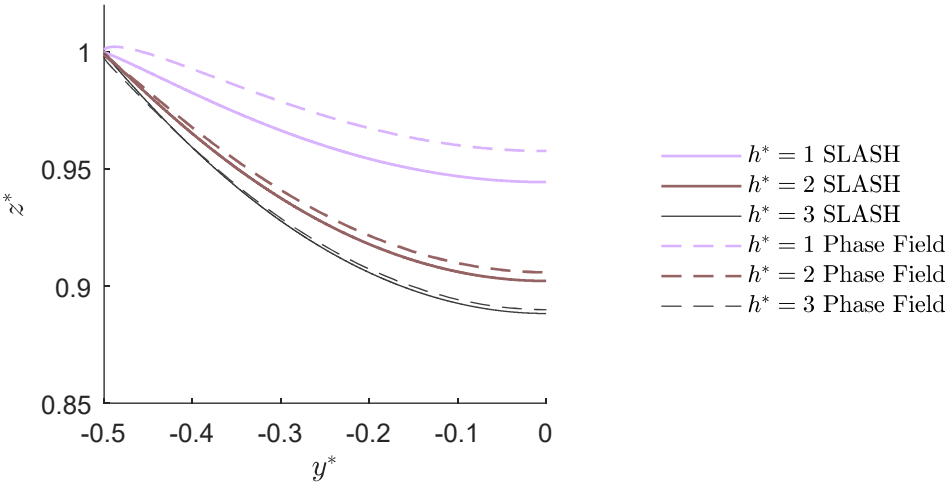

Fig. 7. Evaluation of the meniscus shape for various values of h^*, for $\varepsilon^* = 2$ and $\mathrm{Bo_e} = 10$.

Fig. 8 represents the evolution of the normal electric stress along the interface, as evaluated with the SLASH method. Due to a Taylor cone effect, the normal electric stress is consistently found more important near the edge (Fig. 8), which results in a significant deformation of the interface, especially close to the edge where the sign of the curvature can even change. The apparent angle is also consistently affected in this area. Close to the centre of the interface, far enough from edge effects, the electric stress and the curvature remain constant, allowing to describe the central part of the interface as a circular cap in the presence of an electric stress (Fig. 8). In this area, the consequence of the electric stress only results in a different elevation of the interface, z_0.

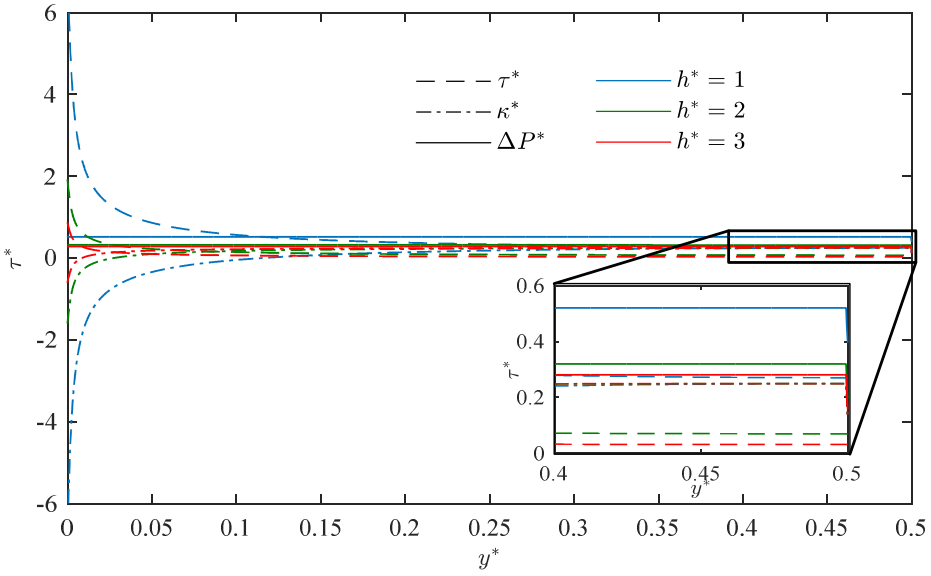

Fig. 8. Electric stress along the interface for various h^* with $Bo = 0.1, Bo_e = 5, \varepsilon^* = 2$ and $\kappa_0^* = 0.25$.

When h^* increases, the normal electric stress becomes more and more homogeneous along the interface (Fig. 8a). As a consequence, a low ratio h^* is recommended to generate a significant impact on the apparent angle.

4.3. Effect of the dielectric permittivity on the normal electric stress

The electric field distribution, and therefore the normal electric stress, are dependent on the permittivities of both media. The location of the meniscus, in other words, the way the media in presence share the available space, also modify the electric field distribution. This two-way coupling leads to a rather complicated impact of the dielectric permittivity on the shape of the meniscus in presence of an electric field. Fig. 9 represents the evaluation of the meniscus shape for various ratio of permittivities, ε^*. The larger the permittivity ratio is, the smaller the normal electric stress experienced by the meniscus is. The latter can even be neglected when $\varepsilon^* > 100$.

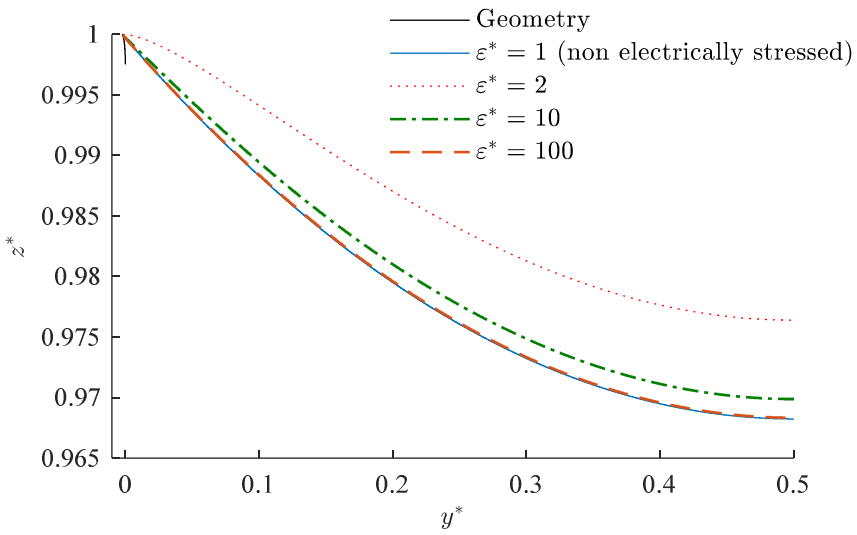

Fig. 9. Shape of the meniscus for various ε^* with $Bo = 0.1$, $Bo_e = 5$, $h^* = 1$ and $\kappa_0^* = 0.25$.

A simplified scheme of the working geometry is represented in Fig. 10: the ground electrode and the high voltage (counter-)electrode are assumed to be infinite and horizontal as well as the liquid-gas interface. This simplified model can be an acceptable approximation of the central area of the meniscus in a working configuration for low h^* values, or equivalently when the width of the groove is larger than the gaseous gap. This configuration enables a direct evaluation of the electric field in the gas phase:

$$E_g^* = \frac{1/h^*}{\frac{1}{h^*\varepsilon^*} + 1}, \tag{21}$$

and the electric field in the liquid phase can be expressed as:

$$E_l^* = \frac{1}{1 + h^*\varepsilon^*} \tag{22}$$

Using Eq. (11), the normal electric stress can be expressed as:

$$\tau_n^* = \frac{Bo_e(\varepsilon^* - 1)}{2h^*}\left(\frac{1}{h^*\varepsilon^* + 1}\right)^2 \tag{23}$$

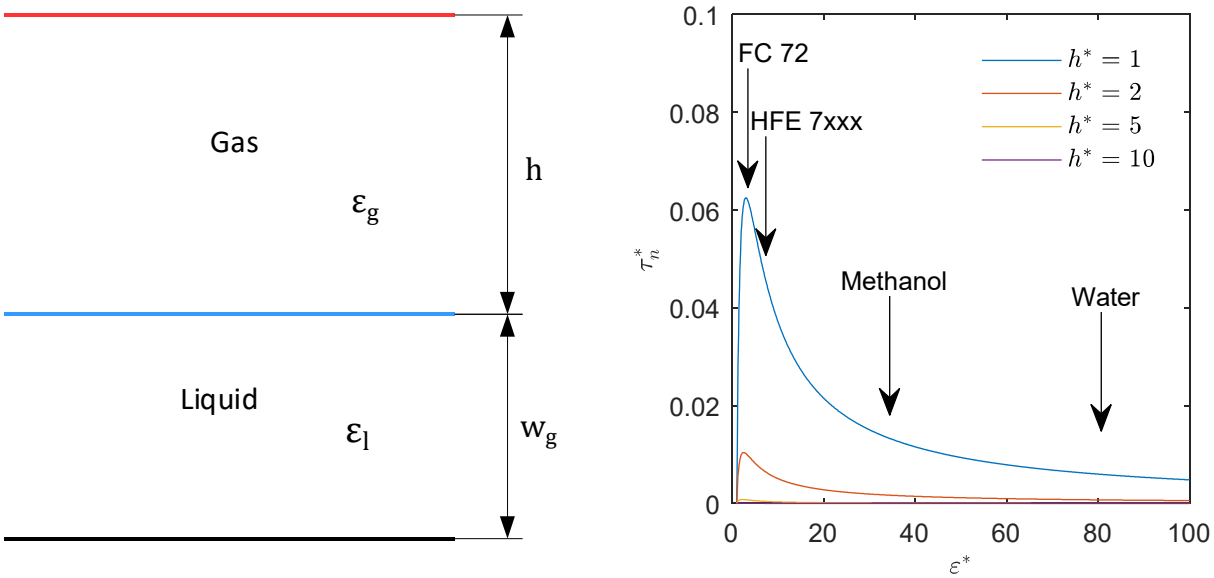

Fig. 10. Simplified scheme of the working geometry (left) and evaluation of the normal electric stress τ_n^* as a function of ε^* and h^* for $Bo_e = 1$ (right).

This simplified configuration allows the comparison of different working fluids for a given gas spacing. Fig. 10 represents the dependence of the normal electric stress τ_n^* on ε^* and h^*. The arrows represent the values of ε^* for common working fluids in equilibrium with their vapour phase. For high h^* values, the liquid phase can be assumed isopotential and the electric stress vanishes in the gas phase due to a large gap . For ε^* close to unity, the two phases can be considered as electrically uniform because of the absence of a jump in electric properties at the interface, which also leads a vanishingly small electric stress. The normal electric stress is maximal for a given h^* if:

$$\frac{\partial \tau_n^*}{\partial \varepsilon^*} = \frac{Bo_e}{2h^*}\left(\frac{1}{h^*\varepsilon^* + 1}\right)^2 + \frac{-2h^* Bo_e(\varepsilon^* - 1)}{2h^*}\left(\frac{1}{h^*\varepsilon^* + 1}\right)^3 = 0. \quad (24)$$

Then, the working fluids give a higher normal electric stress for a given geometry if:

$$\varepsilon^* = 2 + \frac{1}{h^*}. \quad (25)$$

In order to increase the normal electric stress at the centre of the interface, the working fluids must be selected carefully depending on the value of h^*.

4.4. Effect of the Bond number on the meniscus shape

If the width of the groove and the density ratio are large enough, the gravity effect may become as large as the capillary and electric stresses. This leads to a different shape in the absence of electric field: for a low Bond number, the cross section of the interface is well-approximated by a portion of circle but for a high Bond number, the meniscus becomes more sensitive to the gravity in the centre of the groove. Fig. 11 represents the meniscus shape for various Bond numbers. It can be noted that the shape of the interface near the contact angle is significantly governed by the Bond number. Concerning the electric Bond number, the same conclusion holds true.

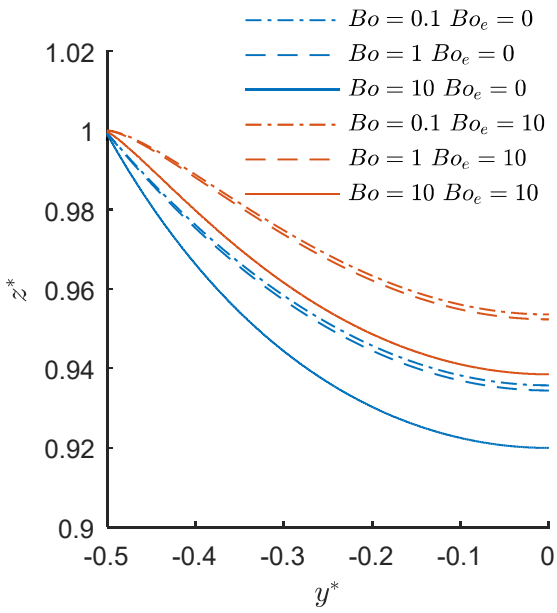

Fig. 11. Meniscus shape for various (Bo, Bo_e) with $h^* = 1$, $\varepsilon^* = 2$ and $\kappa^* = 0.5$.

4.5. Combined effects on the pressure jump

All the previous parameters show various impact on the apparent angle and the pressure jump at the centre of the interface. In order to study the coupled effect of these parameters on the pressure jump and the apparent angle, a large set of dimensionless parameter, $\mathrm{Bo}, \mathrm{Bo_e}, h^*$ and κ^* is studied. Based on section 0, small values of the gaseous gap, h^*, and a small value of the permittivity ratio, $\varepsilon^* = 2$, are selected to get the higher values of the normal electric stress. Fig. 12 represents the dimensionless pressure jump at the centre of the interface as a function of the dimensionless curvature for a large set of the electric Bond number and for different values of the Bond number and the gaseous gap.

The solid blue line represents the analytical solution in the absence of electric field. The numerical solution shows a perfect agreement for this case. The cross markers represent the data as obtained from SLASH method. In the presence of an electric field, the electric Bond number has a major impact on the liquid-gas pressure difference: the higher the electric Bond number, the higher the pressure jump. The normal electric stress can be even greater than the capillary pressure itself. This effect is even more significant for negative values of the curvature (for example, with non-wetting fluids). For high Bond numbers values, the deformation of the meniscus near the edge can not be disregarded and this deformation has a noticeable impact on the meniscus shape in the centre of the groove.

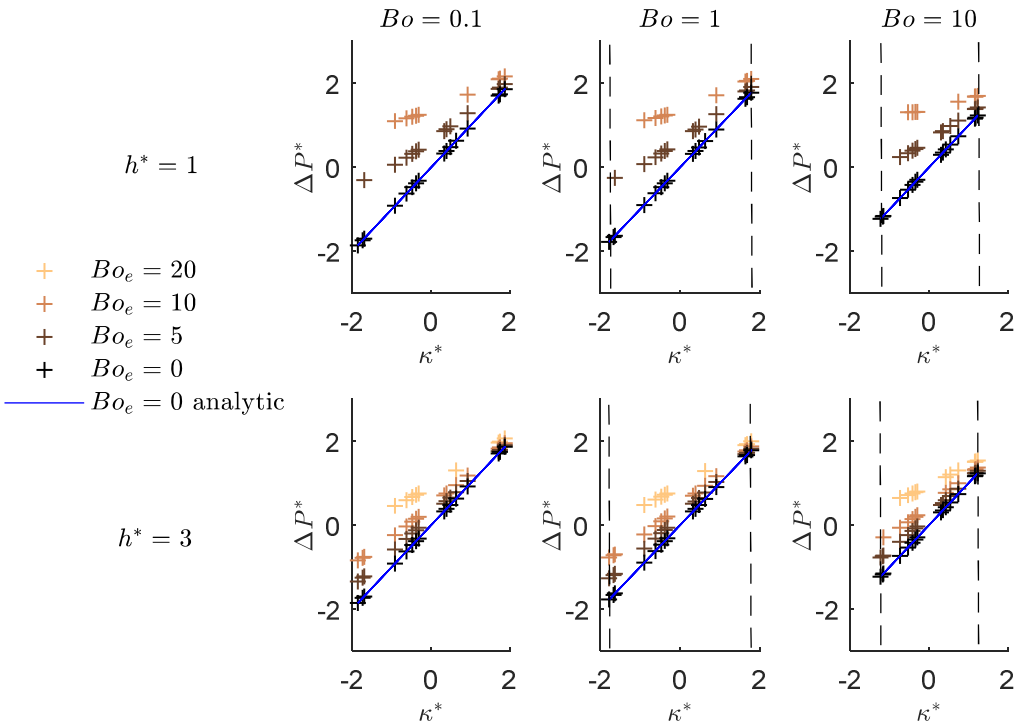

Fig. 12. Pressure jump vs. curvature for various Bond numbers, electric Bond numbers and dimensionless gas spacing with $\varepsilon^* = 2$. Dotted black lines represent the maximal values of κ^*.

As illustrated on Fig. 12, the Bond number has a weak impact on the way the electric stress modifies the meniscus, which means that the gravity effect can be neglected compared to the capillary stress and the normal electric stress at the centre of the interface. But the Bond number has an impact on the extreme values of the curvature that can exist inside the groove (vertical dotted lines on Fig.12). The lower the Bond number is, the greater the maximal curvature achieved at the centre is. Fig. 12 allows the evaluation of the normal electric stress at the centre of the interface. This normal electric stress can be evaluated as the difference between the value of the pressure jump for a given couple $(\mathrm{Bo_e}, \kappa^*)$ and the pressure jump from the analytic solution evaluated in the absence of electric field for the same curvature κ^*. Thus, the effect of the gas spacing on the normal electric stress can be observed. For a gas spacing equal to the dimension of the groove, the electric field is focused near the edges, which results in a noticeable deformation of the interface (Fig. 8). The effect can be so important that the liquid is pulled out of the groove, which leads to the absence of results for $Bo_e = 20$ and $h^* = 1$. For gas spacings greater than the groove, a low variation of the electric field along the liquid-gas interface can be observed, which leads to a smaller deformation of the meniscus shape.

The Bond number and the electric Bond number are two parameters that control the extent of the deformation area. This area is focused near the edge of the grooves, and can be made evident by the variation of the apparent angle. This effect is represented in Fig. 13. On this figure, the apparent angle is plotted as a function of the curvature for various dimensionless numbers.

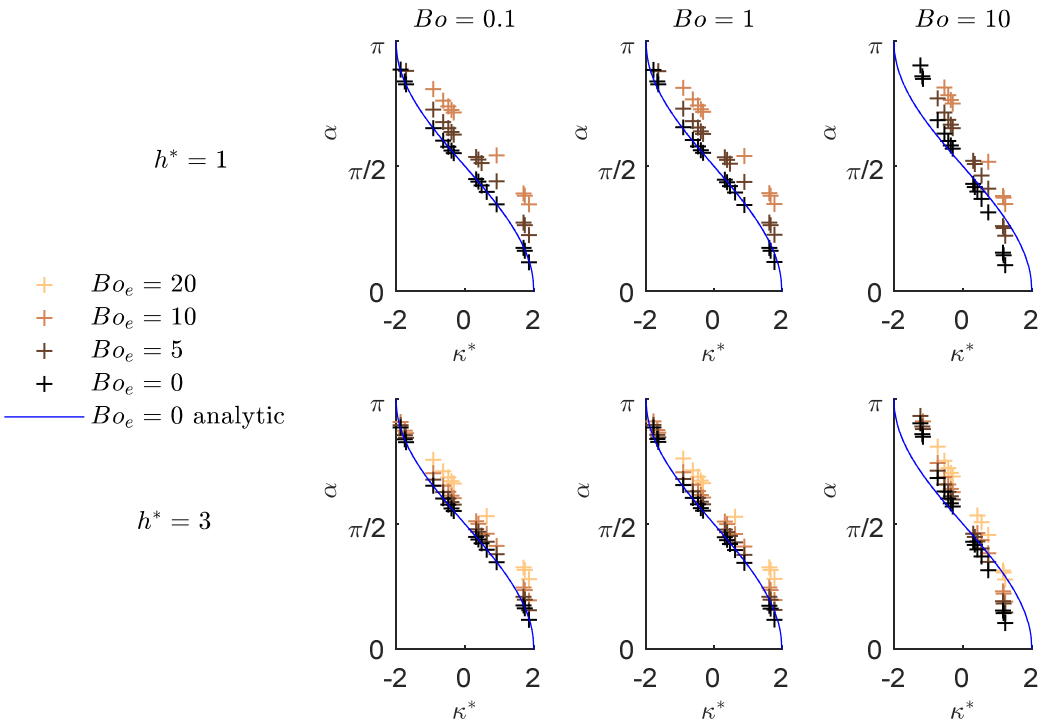

Fig. 13. Evolution of the apparent angle as a function of the curvature for various Bond number, electric Bond number and dimensionless gas spacing ($\varepsilon^* = 2$).

For a given apparent angle, the larger the electric Bond number is, the larger the maximal pressure jump is. This effect is even more important for high absolute values of the curvature. It can be noted that the Bond number has an effect on the apparent angle and it can not be disregarded if the aim is to study the impact of the electric field near the edge. The effect of the gas spacing on the normal electric stress can also be noted: the value of the electric Bond number for $h^* = 3$ is twice the value required to obtain the same pressure jump for $h^* = 1$.

To compare the combined effect of the electric field near the TCL and at the centre of the interface, Fig. 12 and Fig. 13 are combined in Fig. 14. The latter figure represents the dependence of the pressure jump at the centre of the interface on the apparent angle. The solid blue line represents the analytical solution in the absence of gravity and electric field. As seen previously, the normal electric stress at the centre can be evaluated as the difference between the pressure jump evaluated for a given couple ($\mathrm{Bo_e}, \alpha$) and the pressure jump from the analytic solution evaluated in the absence of electric field. The normal electric stress enables to increase the pressure jump at the centre of the interface with the same apparent angle. The lower the apparent angle is, the lower the normal electric stress at the centre of the interface is.

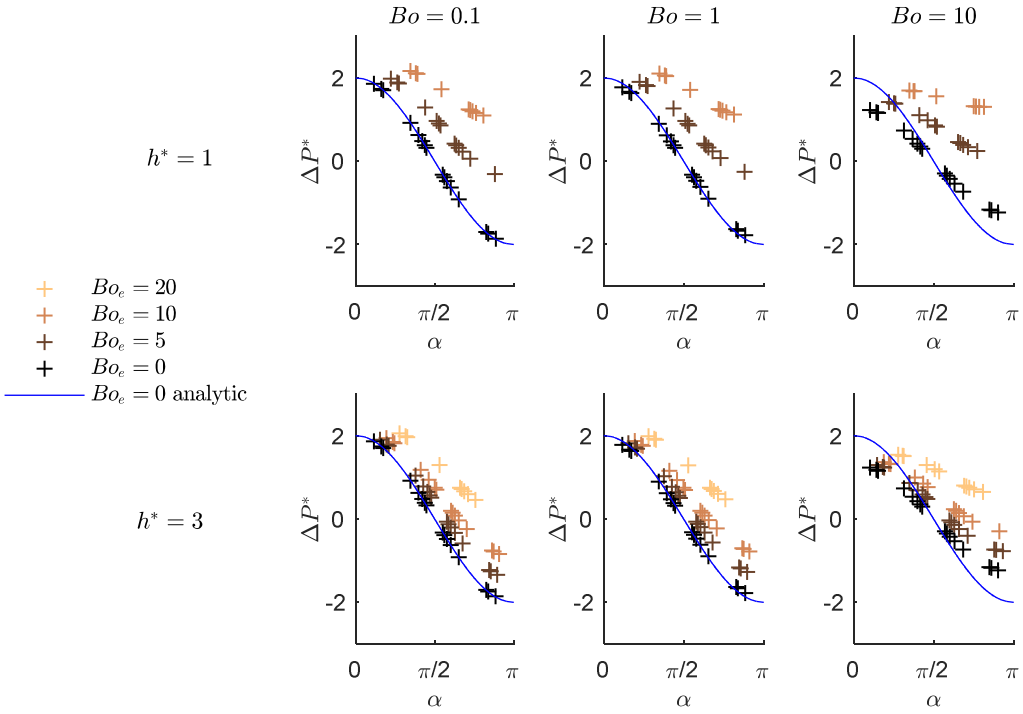

Fig. 14. Evolution of the maximal pressure jump as a function of the apparent angle for various Bond number, electric Bond number and dimensionless gas spacing ($\varepsilon^* = 2$).

The non-dimensional results here obtained from SLASH code can be used as a chart to design an EHD-enhanced capillary structure after the groove geometry or the working fluids have been selected. As demonstrated in this paper, the strong effect of EHD on a non-wetting configuration also allows the user to envisage a wider selection of working fluids, especially those which are commonly not considered in grooved heat-pipes developments due to their poor performances in the absence of electric field.

5. COMPARISON OF THE METHODS

To take into account the two-way coupling between the bulk flow and the interface, a phase-field method based on the full resolution of the Navier-Stokes equation has been developed. As discussed hereafter, the phase-field and SLASH methods give rise to similar results as far as the interface shape is concerned. This indicates that the flow can be calculated independently. This can be explained by calculating three dimensionless numbers based on our standard configuration (for $\mathrm{Bo_e} = 10, \mathrm{Bo} = 0, \mathrm{k}^* = 0.68, \varepsilon^* = 2$):

The capillary number: $\mathrm{Ca_n} = \frac{\mu \frac{\partial v_n}{\partial n}}{\sigma \kappa} \sim 10^{-2} \ll 1$,

The Masson number: $\mathrm{M} = \frac{\varepsilon E^2}{\mu \frac{\partial v_n}{\partial n}} \sim 10^{13} \gg 1$,

The Weber number: $\mathrm{We} = \frac{\rho u_t^2}{\sigma \kappa^2} \sim 10^{-4} \ll 1$.

The fact that $\mathrm{Ca_n}$ remains small while the Masson number M is very large demonstrates that the normal viscous stress does not contribute to the shape of the meniscus, in contrast to other studies devoted for instance to the deformation of a drop in an electric field (Mandal *et al.*, 2014; Bandopadhyay *et al.*, 2016). The fact that the

Weber number, We, also remains very small indicates that the flow, as electrically induced along the interface and viscously propagated into the adjacent volumes, does not generate a pressure gradient along the interface large enough to deform it.

A summary of the respective advantages and disadvantages of the SLASH method and the phase-field method is presented in Table 4. The previous results show that the SLASH method provides the same results at the centre of the groove but a better evaluation of the apparent angle. Due to its independence on the flow, the SLASH method is finally found faster and more robust than the phase-field method, with no compromise on the accuracy, allowing the study of the recession of the contact line. The good evaluation of the apparent angle is important when one wants to study the maximum pressure jump that the capillary structure can sustain, corresponding to the limit of the recession of the meniscus inside the groove, which is directly linked to the apparent contact angle and the grooves geometry. In its current form, the phase field method cannot be used for this purpose. Besides this major drawback, the phase field method also requires to solve the transient Navier-Stokes equations, which leads to a huge CPU time. Moreover, the very different levels of refinement in the meshes used by SLASH and phase field methods strongly impact the calculation time. In order to get a smooth interface, the mesh should be refined on a large extent in the phase field approach. Thus, the transient calculations leads to significant refined area because of the deformation of the interface and finally lead to a significant CPU time. For the SLASH method, the mesh is adapted after each iteration, allowing us to refine the mesh only in the relevant areas. For example, with a CPU i7-4710MQ@ 2.5 GHz, the time to reach a steady solution with the phase-field method is of the order of 10 min while it is of the order of 10 s with the SLASH method. The time efficiency provided by the SLASH method enables the coupling with other phenomena like mass or heat transfers with nevertheless a reasonable calculation time.

Table 4. Advantages and disadvantages of the two methods.

	Advantages	Drawbacks
SLASH	• Very fast • Geometrical boundary condition for the TCL	• Could not be extended to transient problem
Phase-field	• Well known method • Transient regimes can be handled • Calculation of the velocity in both phases is performed	• High computational cost (needs to solve Navier-Stokes equations) • Boundary condition at the TCL is a pointwise stress

6. CONCLUSIONS

A theoretical model was developed to analyse the EHD-induced deformation of a meniscus in a square groove. The model is based on the Laplace-Young equation for the evaluation of the meniscus shape and on the Laplace

equation for the evaluation of the electric potential. The Laplace-Young equation was modified in order to take into account the normal component of the electric stress. The in-house model, referred to as SLASH model, is essentially based on the Gibbs approach for the interfaces (jump notations). It was compared to the phase field method. The SLASH method is found to be significantly faster with an accurate consideration of the boundary conditions. The results show that the electric stress is mostly focused on the edges of the side walls, it can be six-fold larger than its value at the centre of the meniscus when $Bo = 0.1, Bo_e = 5, \varepsilon^* = 2, h^* = 1$ and $\kappa_0^* = 0.25$. The electric stress behaves as a meniscus actuator, especially near the contact line, and it yields higher pressure jumps for a given apparent angle. This last feature possibly enables enhancement of capillary pumping in technological application like heat pipes. Some modifications could be recommended in order to get benefit from the electric actuation of liquid-vapor interfaces with some of the working fluids commonly involved in thermal applications. A thin dielectric layer can be deposited along the surface of the electrodes in order to achieve a net increase of the thermal performances of the system or an AC electric field can be used to lower the impact of the volume density of the electric charges, for instance by adjusting the ratio of the frequency to the RMS value of the electric voltage. Such modifications must be made each time the thermal fluids exhibit a good electrical conductivity, with the aim to avoid the generation of damaging Ohmic currents.

The present theoretical work could be used to design a new EHD-enhanced capillary structure made with square grooves. In that respect, Fig. 12 and Fig. 14 can be considered as useful charts. It must also be noticed that the role of the electric stress is remarkably dependent on the working fluid and the gas space. To reach the higher normal electric stress in a given geometry, a specific working fluid can be used depending of the value of the gas space. A wrong choice of the working fluid could also make the EHD approach to be irrelevant. Further experimental investigations are currently under development in order to validate these theoretical predictions.

The SLASH methodology is here found to be relevant in the case of grooves, especially for the study of meniscus recession, but it can also be used for other type of capillary structures thanks to its ability to calculate the shape of a liquid-gas interface independently from the forces acting on it. Coupled to experimental validations, the fast calculation time and the accuracy of the method can also enable the coupling with different physics, for thermal or chemistry applications for instance.

ACKNOWLEDGEMENTS

The PhD fellowship of N. Cardin is supported by the energy ARC program of Rhône-Alpes region, which is gratefully acknowledged. The financial support of IDEX Université Grenoble Alpes through the IRS program is also acknowledged. The SIMaP laboratory is also part of the LabEx Tec21 (Investissements d'Avenir - Grant Agreement #ANR-11-LABX- 0030).

NOMENCLATURE

a : Numerical parameter for the relaxation time of the director field (m/s)
b : Numerical parameter for the relaxation time of the interface (m^2/s)
e : Unit vector
E : Electric field (V/m)
g : Gravity acceleration (m^2/s)
h : Height of the gas spacing (m)
l : Arbitrary length (m)
n : Normal coordinate (m)
P : Pressure (Pa)
r : Radius of the edge (m)
T : Thickness of the interface (m)
U : Velocity (m/s)
V : Tension (V)
w : Width of the groove (m)
x : Depth coordinate (m)
y : Horizontal coordinate (m)
z : Vertical coordinate (m)

α : Apparent angle (rad)
ε : Permittivity (F/m)
θ : Contact angle (rad)
κ : Curvature (m^{-1})
ϕ : Angle between the tangent at the interface and the horizontal (rad)
ρ : Density (kg/m^3)
ψ : Phase field function
σ : Surface tension (N/m)
σ_e : Electric conductivity (S/m)
τ : Electric stress (N/m^2)

Subscripts
g : Gas
l : Liquid
n : Normal component
t : Tangential component

REFERENCES

Akhlaghi Amiri, H.A., Hamouda, A.A., 2013. Evaluation of level set and phase field methods in modeling two phase flow with viscosity contrast through dual-permeability porous medium. Int. J. Multiph. Flow 52, 22–34.

Atten, P., 2012. Electrohydrodynamics of dispersed drops of conducting liquid: from drop deformation and interaction to emulsion evolution., in: International Symposium on Electrohydrodynamics. Gdansk, Poland.

Bahadur, V., Garimella, S.V., 2008. Energy minimization-based analysis of electrowetting for microelectronics cooling applications. Microelectron. J. 39, 957–965.

Bandopadhyay, A., Mandal, S., Kishore, N.K., Chakraborty, S., 2016. Uniform electric-field-induced lateral migration of a sedimenting drop. J. Fluid Mech. 792, 553–589.

Bryan, J.E., Seyed-Yagoobi, J., 1997. Heat transport enhancement of monogroove heat pipe with electrohydrodynamic pumping. J Thermophys. Heat Transf. 11, 454–460.

Buehrle, J., Herminghaus, S., Mugele, F., 2003. Interface Profiles near Three-Phase Contact Lines in Electric Fields. Phys. Rev. Lett. 91.

Cardin, N., Lips, S., Siedel, S., Davoust, L., Bonjour, J., 2018. Theoretical and experimental investigations of the effect of an electric field on the performance of a grooved flat heat pipe, in: Joint 19th IHPC and 13th IHPS. Pisa, Italy.

Castellanos, A., 1998. Electrohydrodynamics, International Centre for Mechanical Sciences. Springer, Vienna.

Chang, F.L., Hung, Y.M., 2017. Dielectric liquid pumping flow in optimally operated micro heat pipes. Int. J. Heat Mass Transf. 108, 257–270.

Chang, H.-C., 2010. Electrokinetically driven microfluidics and nanofluidics. Cambridge : New-York, p. 508.

Chen, L.-Q., 2002. Phase-Field Models for Microstructure Evolution. Annu. Rev. Mater. Res. 32, 113–140.

Cheng, C.-C., Chang, C.A., Yeh, J.A., 2006. Variable focus dielectric liquid droplet lens. Opt. Express 14, 4101–4106.

Cheng, J.-T., Chen, C.-L., 2010. Adaptive Chip Cooling Using Electrowetting on Coplanar Control Electrodes. Nanoscale Microscale Thermophys. Eng. 14, 63–74.

Cooper, P., 1990. EHD enhancement of nucleate boiling. J. Heat Transf. 112, 458–464.

Darabi, J., Wang, H., 2005. Development of an electrohydrodynamic injection micropump and its potential application in pumping fluids in cryogenic cooling systems. J. Microelectromechanical Syst. 14, 747–755.

Davoust, L., Fouillet, Y., Malk, R., Theisen, J., 2013. Coplanar electrowetting-induced stirring as a tool to manipulate biological samples in lubricated digital microfluidics. Impact of ambient phase on drop internal flow pattern. Biomicrofluidics 7.

Di Marco, P., 2012. The Use of Electric Force as a Replacement of Buoyancy in Two-phase Flow. Microgravity Sci. Technol. 24, 215–228.

Di Marco, P., Kurimoto, R., Saccone, G., Hayashi, K., Tomiyama, A., 2013. Bubble shape under the action of electric forces. Exp. Therm. Fluid Sci. 49, 160–168.

Diao, Y.H., Liu, Y., Zhang, J., Guo, L., Zhao, Y.H., Wang, S., 2015. Effect of electric field on the enhanced heat transfer characteristic of an evaporator with multilayered sintered copper mesh. J. Electrost. 73, 26–32.

Faghri, A., 1995. Heat pipe science and technology, Global Digital Press. ed.

Haeberle, S., Zengerle, R., 2007. Microfluidic platforms for lab-on-a-chip applications. Lab. Chip 7, 1093–1110.

Hallinan, K.P., Bhagat, W., Kashaboina, B., Kashani, A.R., 1998. Electro-hydrodynamic augmentation of heat transport in micro heat pipe arrays. HTD Proc. ASME 361.3, 165–171.

Jones, T.B., 2005. An electromechanical interpretation of electrowetting. J. Micromechanics Microengineering 15, 1184–1187.

Jones, T.B., 1973. Electrohydrodynamic heat pipes. Int. J. Heat Mass Transf. 16, 1045–1048.

Ko, S.H., Lee, S.J., Kang, K.H., 2009. A synthetic jet produced by electrowetting-driven bubble oscillations in aqueous solution. Appl. Phys. Lett. 94.

Liu, Z., Herman, C., Mewes, D., 2006. Visualization of bubble detachment and coalescence under the influence of a nonuniform electric field. Exp. Therm. Fluid Sci. 31, 151–163.

Loehrke, R.I., Sebits, D.R., 1975. Flat plate electrohydrodynamic heat pipe experiments.

Malk, R., Fouillet, Y., Davoust, L., 2011. Rotating flow within a droplet actuated with AC EWOD. Sens. Actuators B Chem. 154, 191–198.

Mancio Reis, F.M., Lavieille, P., Miscevic, M., 2015. Toward enhancement of water vapour condensation using wettability gradient surface. Exp. Therm. Fluid Sci. 67, 70–74.

Mandal, S., Chakraborty, S., 2017. Influence of interfacial viscosity on the dielectrophoresis of drops. Phys. Fluids 29, 052002.

Mandal, S., Chaudhury, K., Chakraborty, S., 2014. Transient dynamics of confined liquid drops in a uniform electric field. Phys. Rev. E 89.

Ogata, J., Yabe, A., 1993. Augmentation of boiling heat transfer by utilizing the EHD effect - EHD behaviour of boiling bubbles and heat transfer characteristics. Int J Heat Mass Transf. 36, 783–791.

Pellat, H., 1896. Électrostatique non fondée sur les lois de Coulomb. Forces agissant sur les diélectriques non électrisés. J Phys Theor Appl 5, 244–256.

Pollack, M.G., Fair, R.B., Shenderov, A.D., 2000. Electrowetting-based actuation of liquid droplets for microfluidic applications. Appl. Phys. Lett. 77, 1725–1725.
Quan, X., Gao, M., Cheng, P., Li, J., 2015. An experimental investigation of pool boiling heat transfer on smooth/rib surfaces under an electric field. Int. J. Heat Mass Transf. 85, 595–608.
Saad, I., Maalej, S., Zaghdoudi, M.C., 2017. Modeling of the EHD effects on hydrodynamics and heat transfer within a fl at miniature heat pipe including axial capillary grooves. J. Electrost. 85, 61–78.
Santra, S., Mandal, S., Chakraborty, S., 2018. Electrohydrodynamics of confined two-dimensional liquid droplets in uniform electric field. Phys. Fluids 30, 062003.
Sharma, R.K., Ganesan, P., Tyagi, V.V., Metselaar, H.S.C., Sandaran, S.C., 2015. Developments in organic solid–liquid phase change materials and their applications in thermal energy storage. Energy Convers. Manag. 95, 193–228.
Shin, W.T., Yiacoumi, S., Tsouris, C., 2004. Electric-field effects on interfaces: electrospray and electrocoalescence. Curr. Opin. Colloid Interface Sci. 9, 249–255.
Siedel, S., Cioulachtjian, S., Robinson, A.J., Bonjour, J., 2016. Lateral coalescence of bubbles in the presence of a DC electric field. Int. Commun. Heat Mass Transf. 76, 127–132.
Siedel, S., Cioulachtjian, S., Robinson, A.J., Bonjour, J., 2011. Electric field effects during nucleate boiling from an artificial nucleation site. Exp. Therm. Fluid Sci. 35, 762–771.
Siva Kumar Gunda, N., Bhattacharjee, S., Mitra, S.K., 2012. Study on the use of dielectrophoresis and electrothermal forces to produce on-chip micromixers and microconcentrators. Biomicrofluidics 6.
Stratton, J.A., 1941. Electromagnetic theory. Mcgraw Hill Book Company, New York and London.
Suman, B., 2006. A steady state model and maximum heat transport capacity of an electrohydrodynamically augmented micro-grooved heat pipe. Int. J. Heat Mass Transf. 49, 3957–3967.
Sun, Y., Beckermann, C., 2007. Sharp interface tracking using the phase-field equation. J. Comput. Phys. 220, 626–653.
Theisen, J., Davoust, L., 2015. Mass transfer enhancement and surface functionalization in digital microfluidics using AC electrowetting: the smaller, the better. Microfluid. Nanofluidics 18, 1373–1389.
Theisen, J., Davoust, L., 2012. Dual-Frequency Electrowetting: Application to Drop Evaporation Gauging within a Digital Microsystem. Langmuir 28, 1041–1048.
Yang, Q., Li, B.Q., Ding, Y., 2013. 3D phase field modeling of electrohydrodynamic multiphase flows. Int. J. Multiph. Flow 57, 1–9.
Yue, P., Zhou, C., Feng, J.J., Ollivier-Gooch, C.F., Hu, H.H., 2006. Phase-field simulations of interfacial dynamics in viscoelastic fluids using finite elements with adaptive meshing. J. Comput. Phys. 219, 47–67.
Zaghdoudi, M.C., Lallemand, M., 2000. Study of the behaviour of a bubble in an electric field: steady shape and local fluid motion. Int. J. Therm. Sci. 39, 39–52.